Coherent far-field excitation of surface plasmons using resonantly tuned metal nanoparticle arrays

Amitabh Ghoshal[*,a], Grady Webb-Wood[a], Clarisse Mazuir[a], and Pieter G. Kik[a,b]
[a]College of Optics and Photonics: CREOL & FPCE, 4000 University Boulevard, University of Central Florida, Orlando, FL 32816, USA;
[b]Physics department, University of Central Florida, Orlando, FL 32816-2700, USA

ABSTRACT

Recent work in plasmon nanophotonics has shown the successful fabrication of surface plasmon (SP) based optical elements such as waveguides, splitters, and multimode interference devices. These elements enable the development of plasmonic integrated circuits. An important challenge lies in the coupling of conventional far-field optics to such nanoscale optical circuits. To address this coupling issue, we have designed structures that employ local resonances for far-field excitation of SPs. The proposed coupler structure consists of an array of ellipsoidal silver nanoparticles embedded in SiO_2 and placed close to a silver surface. To study the performance of the coupler we have performed simulations using the Finite Integration Technique. Our simulations show that normal incidence illumination at a free-space wavelength of 676 nm leads to the resonant excitation of SP oscillations in the Ag nanoparticles, accompanied by coherent near-field excitation of propagating SPs on the Ag film. The excitation efficiency can by maximized by tuning the aspect ratio of the nanoparticles, showing optimum coupling at an aspect ratio of 3.0 with the long axis (75 nm) along the polarization of the excitation signal. We discuss the origin of these observations.

Keywords: nanoparticle, surface plasmon, coupling, efficiency, near-field, array, plasmonics, metal nanophotonics

I. INTRODUCTION

In recent years, surface plasmons (SPs) have gained attention because of the possibility of their application in nanophotonic and plasmonic devices.[1] Surface plasmons are electron charge density waves confined to and traveling along the surface between a metal and a dielectric.[2] SP mode sizes are not intrinsically bound by the diffraction limit, as has been shown in experiments involving propagation of SPs along nanoparticle chains,[3] micro-scale metal strips[4] and nano-scale metal wires.[5] Using propagating SPs on metal surfaces, simple quasi two-dimensional optical circuits have already been demonstrated.[6, 7]

An important challenge in creating integrated plasmonic nanodevices is achieving efficient local excitation of propagating SPs using a structure with a small (few μm^2) footprint. Direct excitation of SPs on a smooth metal surface using free-space illumination is not possible since the SP wavelength is smaller than the corresponding free-space wavelength, resulting in a momentum mismatch between the excitation wave and the SP wave. To overcome this problem SPs are commonly excited by prism-coupling or grating coupling, generally involving weak coupling of light with SPs over a relatively large area, or by near-field excitation, involving relatively strong light-SP coupling using individual nanostructures. Prism coupling makes use of a material with a high refractive index to overcome the momentum mismatch.[2] Grating couplers, on the other hand, make use of a periodic surface structure to overcome the momentum mismatch. Grating coupling has been achieved by either directly structuring the metal surface,[2, 8, 9] or by structuring a thin dielectric layer on the metal surface.[10] Ditlbacher *et al*. measured an excitation efficiency of about 15% using a one dimensional grating with only three periods.[11] In contrast, near-field excitation uses isolated nanostructures for SP excitation. In this case the momentum mismatch is overcome by the existence of high spatial frequency components in the field distribution near the nanostructures. Such near-field excitation has been achieved using different types of nanostructures, including surface relief,[11] nanoscale apertures of various shapes and sizes,[12-14] and particles both on[15, 16] and above[17] a metal surface.

[*] Email: aghoshal@creol.ucf.edu, Web: http://kik.creol.ucf.edu, Phone: +1-407-823-6899

Plasmonics: Metallic Nanostructures and Their Optical Properties III, edited by Mark I. Stockman,
Proceedings of SPIE Vol. 5927 (SPIE, Bellingham, WA, 2005) · 0277-786X/05/$15 · doi: 10.1117/12.617686

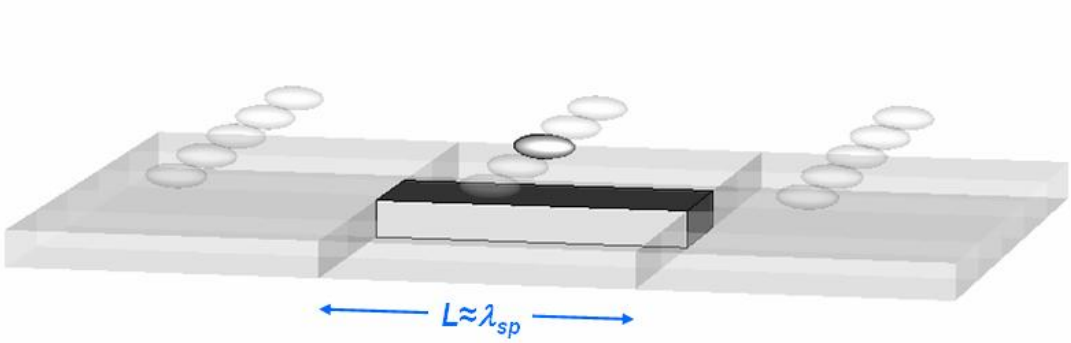

Figure 1. Schematic representation of a nanoparticle enhanced far-field to near-field coupler. A single unit cell is highlighted.

In order to design small coupler structures that efficiently excite surface plasmons one can employ a combination of local field enhancement and coherent excitation. Recent theoretical work on light transmission through periodically structured thin metal films demonstrated one possible approach based on tuning the depth and width of a surface grating.[18] In the present article we discuss an alternative approach to achieving efficient surface plasmon excitation which combines local resonances on metal nanoparticles with coherent plasmon excitation on a metal surface. A sketch of the proposed structure is shown in figure 1. The structure consists of a 2D array of metal nanoparticles embedded in an SiO_2 cladding layer in close proximity to a silver-SiO_2 interface. We will show that resonant excitation of SPs on the metal nanoparticle array results in a periodic and locally enhanced field distribution near the Ag surface, which results in enhanced near-field excitation of propagating SPs. We demonstrate that the SP excitation efficiency can be optimized by tuning the nanoparticle shape. We believe that these nanoparticle enhanced plasmon couplers can play an important role as optical interconnects between far-field optical and integrated plasmon optical circuits.

II. THEORY

As mentioned in the introduction surface plasmons are longitudinal charge oscillations that can exist at a metal surface or at a metal-dielectric interface. The dispersion relation of SPs on an Ag-SiO_2 interface links the plasmon wavelength λ_x to the excitation frequency, and is given by

$$k_x = \frac{\omega}{c}\sqrt{\frac{\varepsilon_{Ag}\varepsilon_{SiO_2}}{\varepsilon_{Ag}+\varepsilon_{SiO_2}}} \tag{1}$$

where $k_x = 2\pi/\lambda_x$ is the plasmon wavevector along the metal surface, ω is the angular frequency, c is the speed of light in vacuum, and $\varepsilon_{Ag}(\omega)$ and $\varepsilon_{SiO_2}(\omega)$ are the dielectric functions of silver and silica respectively. The corresponding surface plasmons have a frequency dependent propagation length L_p given by

$$L_p = \frac{1}{\left|2k_x^{''}\right|} = \frac{c}{\omega}\left(\frac{\varepsilon_{Ag}^{'}+\varepsilon_{SiO_2}}{\varepsilon_{Ag}^{'}\varepsilon_{SiO_2}}\right)^{3/2}\frac{\varepsilon_{Ag}^{'2}}{\varepsilon_{Ag}^{''}} \tag{2}$$

where k_x'' is the imaginary part of the SP wavevector, and ε_{Ag}' and ε_{Ag}'' are the real and imaginary parts of the silver dielectric function. Based on existing literature data[19, 20] for these dielectric functions one finds that SPs excited with light at a free-space wavelength $\lambda_0 = 850$ nm can propagate over a distance of 100 μm, while SPs excited at $\lambda_0 = 1.5$ μm can propagate as far as 390 μm. These types of propagation lengths are sufficiently long to create functional plasmon based optical devices.

The current numerical study involves SP excitation on thin (50 nm thick) Ag films for practical reasons which will be discussed in the section III. In such thin films the dispersion relation is modified with respect to the analytical

theory discussed above due to finite coupling between SPs present at the top and bottom Ag-SiO_2 interfaces.[21, 22] As a result thin films exhibit both symmetric and anti-symmetric plasmon modes, each with their corresponding propagation characteristics. The full dispersion relation in this situation can be found numerically using a method described by Ward *et al*.[23] Figure 2(a) displays the dispersion relation for a 50 nm thick Ag film in SiO_2 found by this method, with the dark lines in the figure corresponding to allowed SP modes. The details of the calculation method used will be discussed in a forthcoming article. As will be shown below, the nanoparticle coupler predominantly excites an asymmetric coupled SP mode. It is anticipated that the main findings of this article will be reproduced on thick Ag films, albeit with slightly modified wavevector values. To enable a direct comparison of our theoretical findings with experiments, we design the coupler structure for operation at $\lambda_0 = 676$ nm (corresponding angular frequency is 2.78×10^{15} rads/sec), as this wavelength can be generated using a Kr ion laser. The corresponding design frequency is indicated in figure 2(a). At this frequency, the SP propagation length on a thick Ag film is predicted to be approximately 65μm.

To excite propagating SPs we will use an array of resonant silver nanoparticles. When illuminated with light at visible frequencies, silver nanoparticles can exhibit a resonantly excited dipolar charge oscillation, known as the Fröhlich mode. Due to the resonant nature of the excitation, the magnitude of the local field strength can exceed the driving field by more than an order of magnitude.[24, 25] For ellipsoidal particles excited along one of their main axes this resonance occurs at a frequency that depends on the aspect ratio of the particle. This is reflected in the particle polarizability given by:[26]

$$\alpha = V\varepsilon_0 \frac{\varepsilon_{Ag} - \varepsilon_{SiO_2}}{\varepsilon_{SiO_2} + F(\varepsilon_{Ag} - \varepsilon_{SiO_2})} \tag{3}$$

where α is the polarizability along the c axis or semi-axis of the nanoparticle, F is a shape-dependent factor ranging from 0 to 1, V is the volume of the particle, and ε_0 is the permittivity of free space. In this study the semi-axes a and b are set equal. The Fröhlich mode occurs at the frequency where the calculated polarizability reaches a maximum. Figure 2(b) shows the calculated resonance frequency of an ellipsoidal Ag nanoparticle in SiO_2 as a function of the aspect ratio c/a. It is found that the nanoparticle resonance coincides with the design frequency of 4.43×10^{14} Hz (corresponding to $\lambda_0 = 676$ nm) for an aspect ratio of $c/a = 3.47$. A second condition that must be satisfied to obtain efficient excitation of propagating SPs is phase matching: SPs excited on adjacent nanoparticles should interfere constructively. This requirement implies that the inter-particle spacing L should be equal to the SP wavelength of the Ag film in SiO_2. From figure 2(a) it can be found that this corresponds to $L = 440$ nm. In the following section we will show that when taking into account the finite coupling between the nanoparticles and the metal surface as well as particle-particle coupling, optimum coupling occurs at a significantly reduced aspect ratio.

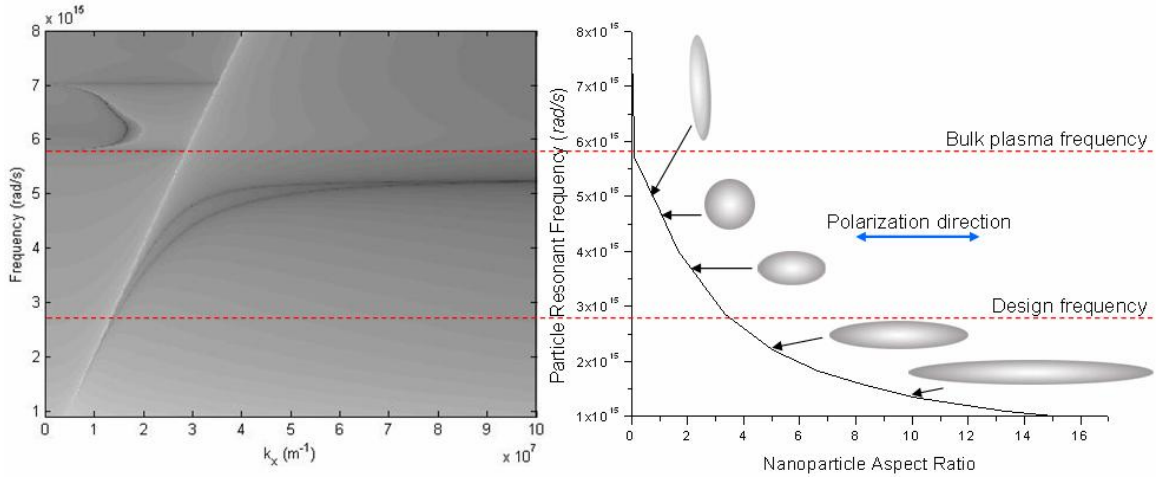

Figure 2(a). Calculated dispersion relation of surface plasmon modes on a 50 nm thick Ag film embedded in SiO_2 based on literature data for the dielectric functions of Ag and SiO_2. The dark lines correspond to allowed SP modes. The white line coincides with the light-line in SiO_2. The splitting of the dispersion curve is caused by coupling of surface plasmons on the front and back of the Ag film. (b) Calculated resonance frequency of an ellipsoidal Ag nanoparticle in SiO_2 as a function of the aspect ratio of the particle.

III. SIMULATION GEOMETRY

To evaluate the performance of the nanoparticle enhanced plasmon coupler we performed numerical simulations using a commercially available 3D electromagnetics simulation package[27] that employs the Finite Integration Technique to model the propagation of electro-magnetic waves in various media. The simulated structure is shown in figure 3. The Ag nanoparticles are located at a height d (surface-to-surface) of 70 nm above the surface of the Ag film. The simulation volume is periodic in the x and y directions, corresponding to an infinite 2D array of nanoparticles above an extended Ag film. The length L of the simulation volume was set to 440 nm, equal to the predicted SP wavelength at the design frequency as discussed in section II. The lateral spacing w between particles was set to 3 times the particle dimension in the y-direction. Note that structures in this size range can be fabricated using existing electron-beam lithography tools. In the following discussion the parameters d, L, and w are held constant, while the particle aspect ratio is varied at constant particle volume. To keep total simulation time at an acceptable level, we chose to simulate a 50 nm thick Ag film embedded in SiO_2 rather than a semi-infinite Ag slab. Under these conditions, individual simulations took 5 hours on a PC running a 3.0 GHz Pentium 4 processor.

The simulated structure is excited with a plane wave that is traveling from the positive z-direction towards the negative z-direction, and is polarized along the x-direction, corresponding to the c-axis of the nanoparticle. To evaluate the performance of the coupler over a finite frequency range, the field amplitude of the plane wave was chosen to have a Gaussian modulated sinusoidal time dependence, corresponding to a short pulse with a Gaussian frequency spectrum centered around 4.43×10^{14} Hz ($\lambda_0 = 676$nm) with a total bandwidth of ±30% in frequency. To monitor the time dependent electric field at various locations in the simulation volume we placed field probes at the locations marked 1, 2, and 3 in figure 3. The simulations were run for a time equal to 10 times the duration of the excitation signal. The mesh density was set to 48 lines per wavelength in each material, and was automatically sub-gridded at regions of rapid field change. The boundaries of the Ag nanoparticle were approximated by a non-orthogonal grid which allows better description of arbitrary curved surfaces on a Cartesian grid compared to a staircase approximation. The typical simulation volume was 440 nm × 100 nm × 250 nm (x × y × z), and contained approximately 800,000 mesh cells. The SiO_2 was modeled as a lossless material with a frequency independent real dielectric constant of 2.1. The Ag layer was modeled as a Drude metal with the frequency dependent permittivity ε described by:

$$\varepsilon_{Ag} = \varepsilon_\infty + \frac{\omega_p}{\omega^2 + i\Gamma\omega} \tag{4}$$

where ε_∞ is the high frequency limit of the relative permittivity ε of the material, ω_p is the bulk plasma oscillation frequency, and Γ is the electron collision frequency in the material. The optimum values of ε_∞ and ω_p were found by fitting to the known dielectric function of silver. Figure 4 shows a comparison between the literature data[19] and the fitted real and imaginary values of ε for Ag as used in the simulation with $\varepsilon_\infty = 3.262$, $\omega_p = 2.196\times10^{15}$ Hz and $\Gamma = 8.856\times10^{13}$ Hz. The modeled real dielectric function of Ag is in excellent agreement with the literature data. The fit overestimates the imaginary part of the dielectric constant. However, this is not expected to significantly affect the obtained resonance frequencies.

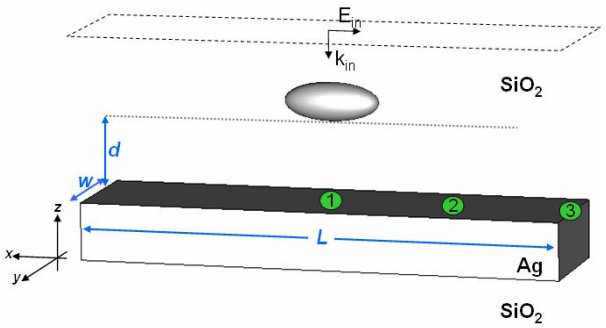

Figure 3. Schematic representation of the simulated structure. The circles marked 1, 2, 3 mark the locations of the time-dependent field probes. Probes 1, 2, and 3 are located on the surface of the Ag film. The x and y boundary conditions are periodic. The structure is excited by a plane wave traveling in the negative z-direction indicated by k_{in}, polarized along the x-direction as indicated by E_{in}.

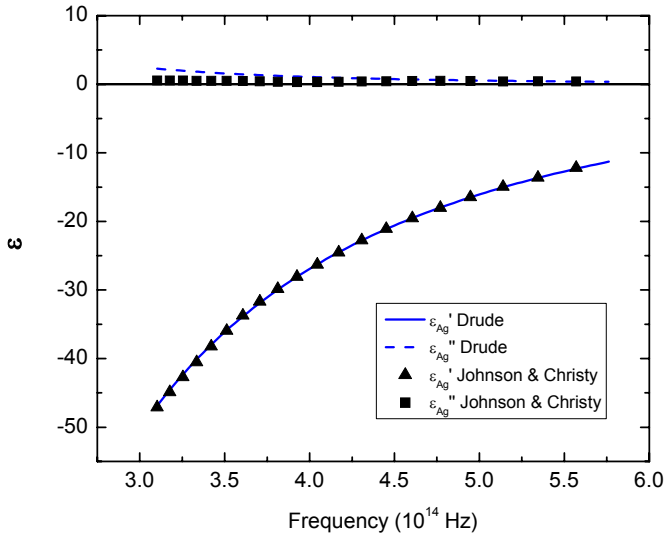

Figure 4. Comparison between dielectric data from literature[19] and the data obtained from the Drude model as used in the simulations. The displayed frequency range corresponds to the bandwidth of the excitation pulse.

IV. RESULTS AND DISCUSSION

Figure 5(a) shows the simulated distribution of the x-component of the electric field (E_x) in the XZ plane during plane wave excitation of a coupler at normal incidence. In this particular example the aspect ratio of the nanoparticles was 2.5. The color scale represents the field amplitude obtained at the design frequency of 4.43×10^{14} Hz, normalized to the excitation amplitude at this frequency. The phase of the plot was optimized for maximum field values. Approximate locations of the corresponding charges responsible for these fields are indicated by the + and – symbols. Note that the E_x field is not constant along the x-direction as might be expected from a plane wave, but instead contains a relatively strong contribution from the silver nanoparticle. Close to the particle the E_x distribution is seen to correspond to a dipolar field distribution. Note that along the silver surface E_x alternates between positive and negative, indicative of the presence of a surface plasmon. The maximum E_x strength near the surface is observed at probe locations 1 and 3. Figure 5(b) shows the corresponding distribution of the E_z field component at the same frequency and phase. The normal E-field components (E_z) present at the silver surface indicate the presence of a surface plasmon. This SP related normal field component is maximum at probe location 2. Note that although the optical transmission of a 50 nm thick Ag film is less than 1%, a significant E_z amplitude (maximum amplitude of 1.9 V/m) is observed at the lower Ag-SiO_2 interface. This is a consequence of coupling between SPs on the top and bottom interface, as discussed in section II.

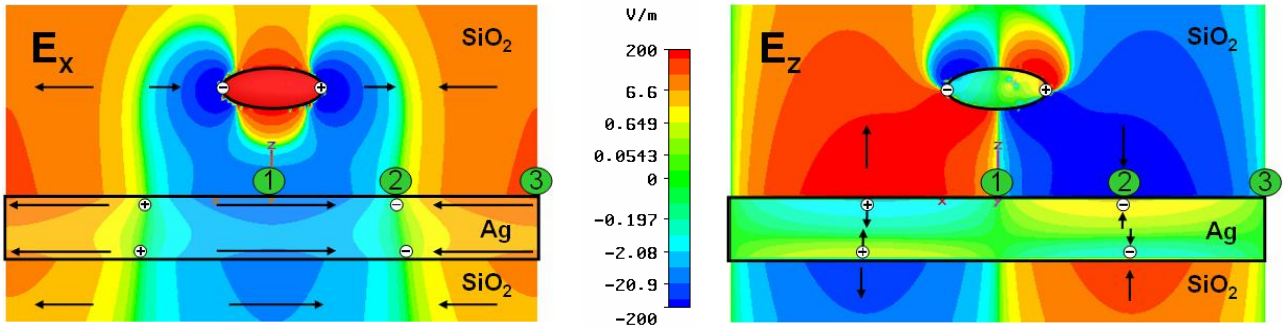

(a) (b)

Figure 5. XZ cuts of the simulation volume at y = 0 showing (a) E_x and (b) E_z response normalized to the driving field amplitude. The color scale indicates the field strength. The arrows represent the general field direction, and the + and – symbols represent regions of high charge density. The locations marked 1, 2, and 3 indicate the position of the time dependent E field probes.

Figure 6(a) shows the time dependent field strength of the incident plane wave applied to the top of the simulation volume (150nm above the Ag surface). Figure 6(b) shows the E_z field observed at probe 2 for a particle aspect ratio of 2.5. Note that a finite E_z amplitude is observed at the silver surface well after the excitation signal has gone to zero, showing that energy is stored in a confined surface plasmon mode. It should be mentioned that part of the energy stored in this surface mode couples back into radiation modes due to the presence of the coupling structure.

The time dependent signal shown in figure 6(b) contains information about the resonant behavior of the structure under investigation. At the location of probe 2, the observed fields consist of the z-component of the SP related electric field and a small contribution due to E_z associated with the dipolar field around the nanoparticle. There is no direct E_z contribution from the incident plane wave excitation field since the incident field is purely x-polarized. Consequently the signal observed at probe 2 represents predominantly the amplitude of the excited surface plasmon. Figure 7 shows the normalized Fourier transforms of the time domain E_z signal at probe 2 for aspect ratios in the range 1.0 to 4.0. To highlight the frequency dependent response of the structure, each curve in figure 7 represents the Fourier transform of the time dependent field at probe 2 divided by the Fourier transform of the excitation pulse.

Several features are evident in figure 7. First, for all aspect ratios a resonance peak is observed around 4.3×10^{14} Hz, corresponding to a free-space wavelength of 697 nm. This is attributed mainly to the periodicity of the structure along the x-direction. Individual nanoparticles in the 2D array launch SP waves propagating along the positive and negative x-direction. These SP waves interfere constructively when the effective SP wavelength matches the inter-particle spacing resulting in an enhanced SP amplitude at a frequency of 4.3×10^{14} Hz. Note that this phase matching occurs at a frequency that is 3% lower that the design frequency. This shift is attributed to the presence of the Ag nanoparticles, which is not taken into account in the calculated SP dispersion relation shown in figure 2(a). Second, the magnitude of the E_z field peak changes as the aspect ratio of the nanoparticle is varied, reaching a maximum at an aspect ratio of 3.0. Note that the normalized field values are larger than 1, indicating field enhancement. Third, as the aspect ratio is increased, a small secondary peak is seen to move from high to low frequencies. This second resonance feature is attributed to the nanoparticle plasmon resonance. At frequencies close to the nanoparticle resonance, an enhanced E field builds up around the particle, in turn resulting in an enhanced SP excitation and a stronger E_z field at Probe 2 at these frequencies. For example, at an aspect ratio of $c/a = 2$ this resonance is found to occur at a frequency near 5.4×10^{14} Hz. As the aspect ratio of the particle is increased, this resonance peak is seen to shift to lower frequencies, as expected based on figure 2(b). When the nanoparticle resonance overlaps with the resonance associated with phase matching, a maximum SP field is obtained. This maximum occurs at a nanoparticle aspect ratio of 3.0, which is significantly lower than the predicted aspect ratio of 3.5 that was obtained based on figure 2(b). This difference is attributed to the coupling between propagating light, local nanoparticle resonances, and propagating SPs which was not taken into account in figure 2(b).

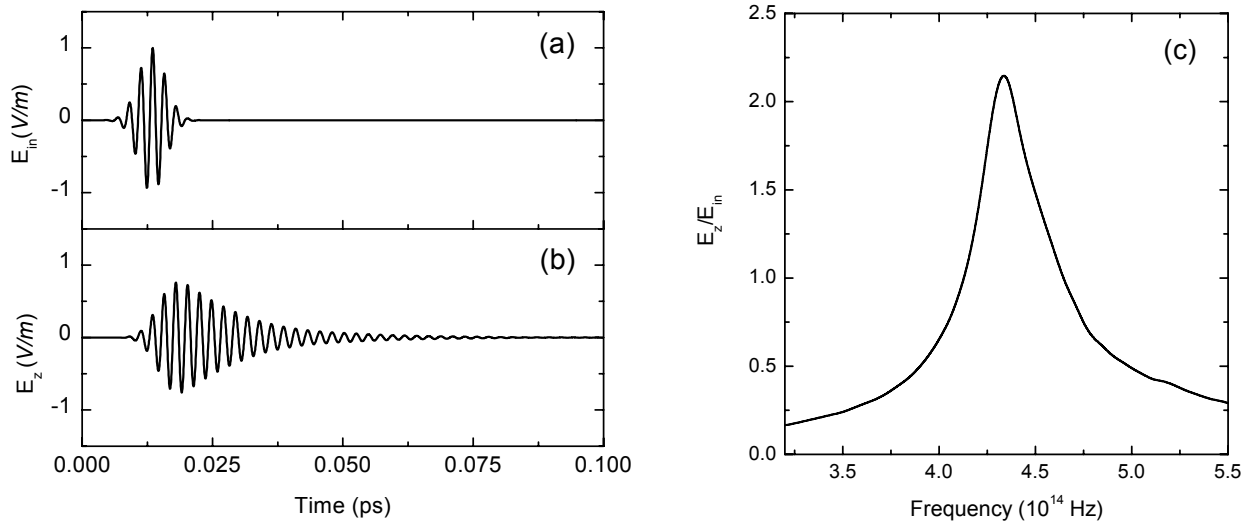

Figure 6. (a) Time dependence of the excitation signal. (b) Time dependent E_z response detected at probe 2 resulting from the excitation signal in figure 4(a) for a coupler structure containing nanoparticles with an aspect ratio of 2.5. (c) Normalized Fourier transform of the time domain signal shown in (b).

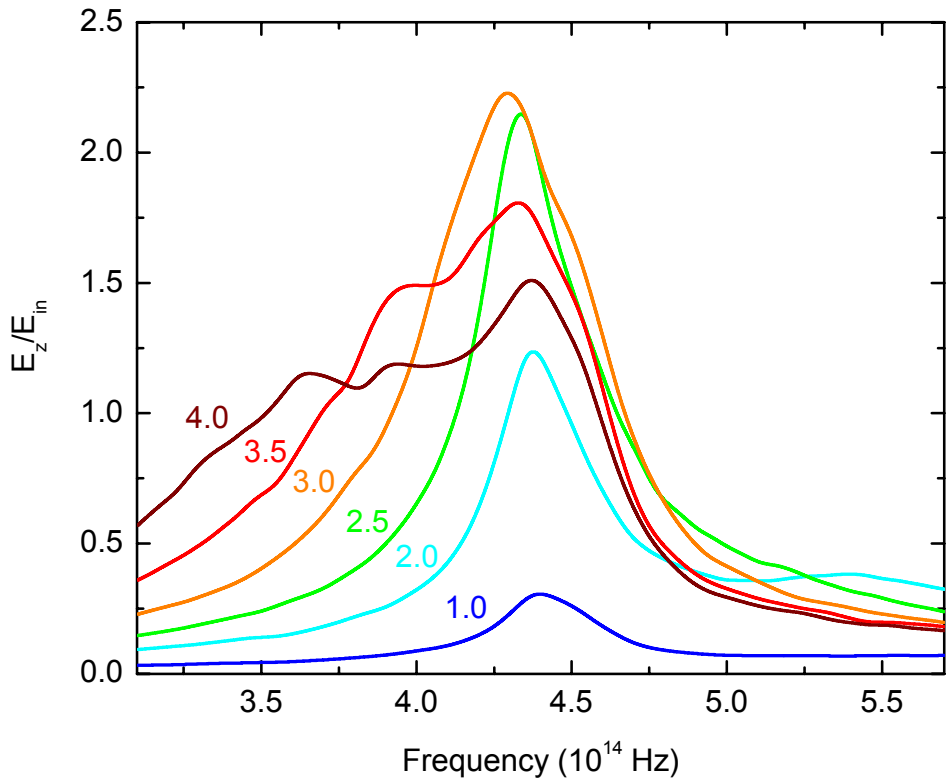

Figure 7. Normalized Fourier transforms of $E_z(t)$ detected at probe 2 for nanoparticle aspect ratios in the range 1.0-4.0. Optimum surface plasmon excitation is observed at an aspect ratio of 3.0.

V. CONCLUSION

We have investigated a metallic structure designed to convert far-field radiation into propagating surface plasmons mediated by plasmon resonances on metal nanoparticles. It is shown that a 2D array of Ag nanoparticles (75 nm long, 30 nm wide) can be used to excite surface plasmons at an Ag-SiO_2 interface using normal incidence illumination. The surface plasmon excitation efficiency under illumination at 676 nm was optimized by matching the inter-particle spacing to the plasmon wavelength, while tuning the nanoparticle aspect ratio. Optimum surface plasmon excitation was obtained when the nanoparticle resonance frequency coincided with the SP frequency, which occurred at a nanoparticle aspect ratio of 3.0. This type of resonantly tuned coupler structure could play an important role in integrated plasmonic circuits.

VI. REFERENCES

1. Barnes, W.L., A. Dereux, and T.W. Ebbesen, *Surface plasmon subwavelength optics.* Nature Materials, 2003. **424**(6950): p. 824.
2. Raether, H., *Surface Plasmons on Smooth and Rough Surfaces and on Gratings.* Springer Tracts in Modern Physics, 1988. **111**.
3. Maier, S.A., et al., *Local detection of electromagnetic energy transport below the diffraction limit in metal nanoparticle plasmon waveguides.* Nature Materials, 2003. **2**(4): p. 229.
4. Lamprecht, B., et al., *Surface plasmon propagation in microscale metal stripes.* Applied Physics Letters, 2001. **79**(1): p. 51.
5. Schider, G., et al., *Plasmon dispersion relation of Au and Ag nanowires.* Physical Review B (Condensed Matter and Materials Physics), 2003. **68**(15): p. 155427.
6. Ditlbacher, H., et al., *Two-dimensional optics with surface plasmon polaritons.* Applied Physics Letters, 2002. **81**(10): p. 1762.
7. Hohenau, A., et al., *Dielectric optical elements for surface plasmons.* Optics Letters, 2005. **30**(8): p. 893.
8. Dmitruk, N.L., et al., *On a control of photon-surface plasmon coupling at a multilayer diffraction grating.* ASDAM Conference Proceedings. Third International EuroConference on Advanced Semiconductor Devices and Microsystems, 2000: p. 445.
9. Watts, R.A., A.P. Hibbins, and J.R. Sambles, *The influence of grating profile on surface plasmon polariton resonances recorded in different diffracted orders.* Journal of Modern Optics, 1999. **46**(15): p. 2157.
10. Hibbins, A.P., J.R. Sambles, and C.R. Lawrence, *The coupling of microwave radiation to surface plasmon polaritons and guided modes via dielectric gratings.* Journal of Applied Physics, 2000. **87**(6): p. 2677.
11. Ditlbacher, H., et al., *Efficiency of local light-plasmon coupling.* Applied Physics Letters, 2003. **83**(18): p. 3665-3667.
12. Jin, E.X. and X. Xu, *Radiation transfer through nanoscale apertures.* Journal of Quantitative Spectroscopy and Radiative Transfer, 2004. **93**(1-3): p. 163.
13. Guo Ping, W., Y. Yongxiang, and W. Bing, *Evanescent coupling of transmitted light through an array of holes in a metallic film assisted by transverse surface current.* Journal of Physics (Condensed Matter), 2003. **15**(47): p. 8147.
14. Thio, T., et al., *Enhanced light transmission through a single subwavelength aperture.* Optics Letters, 2001. **26**(24): p. 1972.
15. Ditlbacher, H., et al., *Fluorescence imaging of surface plasmon fields.* Applied Physics Letters, 2002. **80**(3): p. 404.
16. Hecht, B., et al., *Local excitation, scattering, and interference of surface plasmons.* Physical Review Letters, 1996. **77**(9): p. 1889.
17. Kume, T., et al., *Interaction between localized and propagating surface plasmons: Ag fine particles on Al surface.* Solid State Communications, 1995. **93**(2): p. 171.
18. Garcia-Vidal, F.J., et al., *Multiple paths to enhance optical transmission through a single subwavelength slit.* Physical Review Letters, 2003. **90**(21): p. 213901.
19. P. B. Johnson and R. W. Christy, Phys. Rev. B 6, 4370 (1972).
20. E. D. Palik, Handbook of Optical Constants (Academic, London, 1985).
21. Sarid, D., *Long-range surface-plasma waves on very thin metal films.* Physical Review Letters, 1981. **47**(26): p. 1927.
22. Burke, J.J., G.I. Stegeman, and T. Tamir, *Surface-polariton-like waves guided by thin, lossy metal films.* Physical Review B (Condensed Matter), 1986. **33**(8): p. 5186.
23. Ward, C.A., et al., *Multimedia dispersion relation for surface electromagnetic waves.* Journal of Chemical Physics, 1975. **62**(5): p. 1674.
24. Boyd, G.T., Z.H. Yu, and Y.R. Shen, *Photoinduced luminescence from the noble metals and its enhancement on roughened surfaces.* Physical Review B (Condensed Matter), 1986. **33**(12, Part 1): p. 7923.
25. Mohamed, M.B., et al., *The 'lightning' gold nanorods: fluorescence enhancement of over a million compared to the gold metal.* Chemical Physics Letters, 2000. **317**(6): p. 517.
26. Bohren, C.F. and D.R. Huffman, *Absorption and Scattering of Light by Small Particles.* 1998.
27. Computer code Microwave Studio 5, Computer Simulation Technology, Darmstadt, Germany.